doi:10.1038/nature11789

Content

1.NEEM measurements used in this study

1.1 Stable water isotopes (University of Copenhagen and Labatorie des Sciences du Climat et de l'Environment in Sacley)

55 cm samples from the NEEM ice core (0-2537 m) have been measured for the stable water isotope $\delta^{18}O_{ice}$ at the Centre for Ice and Climate, Niels Bohr Institute[51] and at Labatorie des Sciences du Climat et de l'Environment in Sacley using mass spectrometry with an accuracy better than 0.1 ‰ [52]. The 5 cm samples have been measured from 2186 to 2210 m at the Centre for Ice and Climate, Niels Bohr Institute using cavity ring-down spectroscopy with an accuracy of approx. 0.1 ‰.

The measurements from 2162.1 m to 2533.3 m are used in the reconstruction of the last interglacial, the Eemian.

Data file: NEEM_O18ice_Nature2012.xls

1.2 N_2O, CH_4 and air content (University of Bern)

Discrete ice samples with a length of 3 cm taken from the deepest part of the NEEM ice core (2201 to 2519 m, 278 measurements) have been measured for CH_4 and N_2O concentrations at the Division for Climate and Environmental Physics, Physics Institute, University of Bern. The air is extracted in a melt-refreeze step[5,53-55] and analyzed by gas chromatography with a mean uncertainty of 10 ppbv for CH_4 and 5 ppbv for N_2O. Note that we apply an offset correction of +10 ppbv to the measured N_2O concentrations to be consistent with earlier measurements[5,55,56]. After completion of the melt-refreeze step and before the analysis in the TCD, FID, and ECD detectors, the extracted air is expanded into a temperature controlled sampling loop (-60°C) and the pressure is measured to determine the total air content of a sample. However, we have no exact temperature information from other parts of the total expansion volume, namely the headspace volume of the extraction containers and the connection to the sampling loop, which induces a systematic offset to the absolute value of our air content measurements. Note that the unknown temperature might also vary with time and between the different extraction containers. Comparison with the calibrated STAN values (see section 1.4) shows that on average the Bern values are 3.5 ml/kg lower. We therefore correct all Bern air content values with this mean offset correction of +3.5 ml/kg.

To obtain a reference air content value during the Holocene, we analyzed 9 additional samples from the NEEM ice core in a depth interval from 103 to 1404 m.

Data file: NEEM_CH4_N2O_AIR _Nature2012.xls

1.3 $\delta^{15}N$, $\delta^{18}O_{atm}$ (CEA)

At the Laboratoire des Sciences du Climat et de l'Environnement, CEA-CNRS-UVSQ, IPSL, 158 duplicate measurements of $\delta^{15}N$ and $\delta^{18}O$ were performed on the air trapped in the NEEM ice core between 2201 and 2524.5 m depth and 5 between 396.3 and 415.5m depth with an associated uncertainty of 0.006‰ and 0.015‰ respectively. The air was extracted with a melt-refreeze method and analysed on a mass spectrometer (Thermo Delta V). Corrections were applied for the influence of the formation of CO^+ of masses 28 and 29 in the mass spectrometer source[23]. Moreover, we measured systematically $\delta O_2/N_2$ for each sample (analytical uncertainty of 0.5‰) to correct for the influence of the ratio O_2/N_2 on the sensitivity of the mass spectrometer source[23]. A detailed description of the method is given in[57].

To obtain the $\delta^{18}O_{atm}$ profile, we corrected the $\delta^{18}O$ of O_2 for physical fractionation processes in the firn (the shallow part of the ice sheet where the porous snow pack has not yet been compressed to impermeable glacier ice). These fractionation processes are driven either by the Earth's gravity field or a temperature gradient within the firn column. The gravitational effect is proportional to the mass difference between the two isotopes[58] . It is therefore twice as large for $\delta^{18}O$ ($^{18}O/^{16}O$) than for $\delta^{15}N$ ($^{15}N/^{14}N$). $\delta^{18}O_{atm}$ is therefore traditionally estimated from the combined measurements of $\delta^{18}O$ and $\delta^{15}N$ as $\delta^{18}O_{atm} = \delta^{18}O - 2\delta^{15}N$ and the final associated uncertainty on $\delta^{18}O_{atm}$ is 0.02‰.

Data file: NEEM_15N_O18atm _Nature2012.xls

1.4 STAN air content (LGGE)

Measurements of air content along the NEEM ice core have been performed at LGGE using an original barometrical method implemented with an experimental setup called STAN[59]. The STAN allows precise evaluation of the pressure and temperature of air extracted from an ice sample by its melting and –refreezing of the sample under a vacuum in a volume-calibrated cell. After correcting both the measured pressure for the partial pressure of saturated water vapor and of the calibrated volume for the volume occupied by refrozen bubble free ice, the air content V is calculated using the ideal gas law.

The ice samples used in STAN have a mass of about 25 g and a regular shape of a rectangular parallelepiped or cube, which facilitates estimation of their specific surface. The latter is needed to correct V measurements for "cut-bubble effect", which is the gas loss from air inclusions (bubbles, gas hydrates and relaxation features such as air cavities) cut at the surface of the sample. The correction depends on the specific surface of the ice sample and the size of air inclusions [60]. The size of air inclusions has been measured under a binocular microscope in 2-4 mm thick sections of ice cut in parallel with the samples used for air content measurements.

The absolute precision of the STAN measurements has been estimated to be within ± 0.6%. However, the overall error of the obtained V values amounts to 1% due to the uncertainties in the cut-bubble correction[59]. The average reproducibility of the STAN measurements performed in the same horizontal slice of an ice core has been confirmed to be better than 1%.

Data file: NEEM_STAN_AIR _Nature2012.xls

1.5 Noble gasses (UC San Diego)

Selected NEEM ice core samples between 2398 and 2404 m (within the Eemian section) were measured for Kr/Ar and Xe/Ar ratios, in order to obtain evidence for melt layers. The experimental technique follows Headly (2008) with minor modifications to reduce sample size. An ice core sample of typically 30-35 g was cut and placed in a chilled glass vessel with two stir bars. The vessel was attached to a vacuum line and pumped out for 40 minutes to remove ambient air and clean the ice surface. The vessel was then disconnected from the pump and warmed to melt the ice. The air released from the ice core was transferred to a dip tube at 4K, after passing through a water trap. The melt water was agitated by stir bars during the transfer, to ensure degassing of Kr and Xe. The gas sample was then gettered for 10 minutes with Zr-Al alloy (SAES st101) to remove reactive gases and heated to 900 ˚C, and remaining noble gases were transferred to another dip tube at 4K. Ultrahigh-purity nitrogen was subsequently added to the sample gas at a pressure approximately 20 times that of the noble gas pressure, in order to increase the total gas amount for mass spectrometry. The sample is then analyzed on a mass spectrometer (ThermoFisher MAT 253) to determine δKr/Ar and δXe/Ar by peak-jumping. The results are standardized against modern air collected from the Scripps pier in La Jolla, USA. The measured δKr/Ar and δXe/Ar were corrected for pressure imbalance and for difference in nitrogen abundance between the sample and reference gases in the mass spectrometer. The overall reproducibility of the measurements is better than 1 and 3 ‰ for δKr/Ar and δXe/Ar, respectively.

1.6 Radio echo sounding data (University of Kansas)

The radio echo sounding data were collected with the CReSIS Multi-channel Coherent Radar Depth Sounder/Imager (MCoRDS/I) onboard the NASA P-3B aircraft during the NASA Operation Ice Bridge 2011 (http://nsidc.org/data/icebridge/index.html). The MCoRDS/I is operated with a 15-element antenna array. The central 7 elements of the array are used to transmit and all 15 elements are used to receive. Two tapered chirp waveforms of 1 μs and 10 μs duration and peak power of about 450 W are transmitted at a pulse repetition frequency of 12 KHz. Both chirps' bandwidth is 30 MHz at a center frequency of 195 MHz. The short 1-μs waveform is used to detect the air-ice interface and map shallow layers in the top 500 m of ice. The longer 10-μs waveform is used to map deep layers and sound the ice-bed interface. Received signals from the 15 antenna elements are digitized, coherently integrated, and stored for further processing. In post processing, the digitized data are pulse compressed with an optimized window to shape the amplitude spectrum of the received signals for reducing range sidelobes to more than 50 dB below the main lobe. This is

done to ensure that the deep internal layers' echoes are not masked by the range sidelobes of the strong ice-bed echoes. At this stage, the pulse-compressed data are migrated. This is equivalent to Synthetic Aperture Radar (SAR) processing of data to improve both along-track resolution and the signal-to-noise ratio. The final step combines the receive channels after compensating for channel differences in magnitude and time delay. To reduce fading resulting from coherent processing of the radar data, 11 along-track samples are incoherently integrated. The final product has a range resolution of 4.5 m in ice, a relative permittivity of 3.15, and an along-track resolution of 30 m.

2. Upstream corrections

When reconstructing past climate conditions from ice core data, upstream corrections of the ice core measurements are needed because the site of ice deposition has been upstream along the line of ice flow leading to the ice core site. Typically, the depositional sites have been at a higher elevation and at a different geographic position and upstream corrections are needed if the ice core data are to be interpreted as climate records. The surface elevation differences include both an elevation difference simply because the site is upstream and a term from a difference in size and shape of the ice sheet back in time. The locations of the depositional sites need to be calculated from an ice sheet flow model. Present day surface elevation at the depositional location is obtained from the observed surface elevations[33]. The local elevation change is constrained by the air content of the ice core data itself. Using a nested 3-dimensional flow model[34] that takes into account higher-order stresses, a Lagrangian backtracing on a 2.5 km grid with 100 layers in the vertical direction is used to reconstruct the depositional locations of the ice found in the NEEM ice core as a function of time (Figure 1a). The 128 kyr BP old ice is found to originate at a location that is about 205 km upstream and 330 m higher than the present elevation of the surface at NEEM[33]. While differences occur in the extent of the reconstructed Eemian ice sheet[34,61], such variations had only a limited effect on the shape of the ice sheet and the ice divide position upstream of the NEEM site. The location of the depositional sites only depends on the history of the flow velocity during the period the ice traveled since it was deposited. The nested 3 dimensional model simulates current surface velocities around the NEEM site well. In the absence of major changes in the ice sheet shape around the ice core site, time-dependent changes in the flow velocity along the ice divide scale with changes of the accumulation rate, which are equally known from the ice core results. As an example of the robustness of the upstream advection correction, a more simple approach that uses the present fixed ice ridge as the flow line and using simple Dansgaard-Johnsen velocity profiles reaches the same results with a depositional site of the 130 kyr BP old ice 180 km upstream and 300 m higher than the

present surface elevation of NEEM[62]. At NEEM, the present mean annual surface temperature is -29°C[63], the mean of the accumulation for the last 1000 years is 0.220 ± 0.05 m ice equivalent/ year[8] and the present horizontal surface velocity is 5.8 ± 0.3 m/yr[64]. Both models are tuned to these observed values.

3. Corrections of the stable water isotopes

As presented in the Supplementary Information of [32] the relationship between surface temperature change and measured $\delta^{18}O_{ice}$ change in the present interglacial 11.700 years before year AD2000 (b2k) is given by the following equation:

$$\Delta T = 2.1 \, (\, \Delta\delta \, + 0.0062 \, \Delta S_{elevation} + [0.0062 \, \Delta S_{upstream} + 0.48 \, \Delta L + \Delta\delta_{SEA}] \,) \qquad \text{(SE1)}$$

where $\Delta\delta$ is the change of $\delta^{18}O_{ice}$ values, $\Delta S_{upstream}$ is the recent difference in altitude between the present surface elevations of the NEEM site and the upstream depositional site, $\Delta S_{elevation}$ is the elevation related to a change in the size and shape of the ice sheet (local elevation change), ΔL is the latitude change and $\Delta\delta_{SEA}$ is the change of the $\delta^{18}O$ of the ocean water[65]. The correction to apply

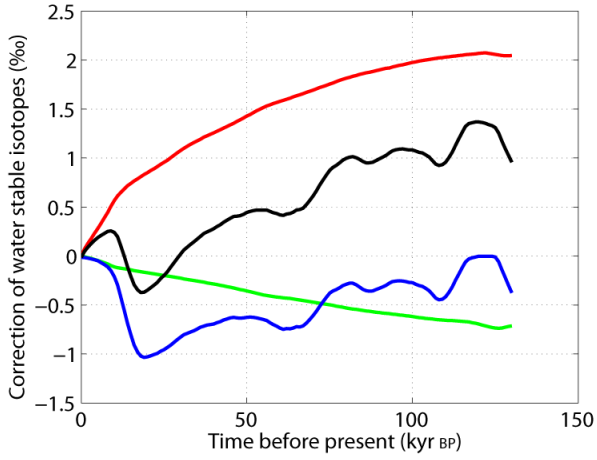

Figure S1: Corrections of the stable water isotopes $\delta^{18}O_{ice}$. The $\delta^{18}O_{ice}$ values measured in the NEEM ice core need to be corrected for changing values of the $\delta^{18}O$ of ocean water (SMOW) with time (blue)[65], the changing latitude of the depositional site (green) and the upstream change of the present surface elevation at the depositional site (red) before it can be interpreted as a temperature proxy on the evolving surface at the NEEM site. The black curve represents the sum of the corrections.

before discussing local elevation changes and temperature changes is:

$$\text{Correction} = [0.0062\ \Delta S_{upstream} + 0.48\ \Delta L + \Delta\delta_{SEA}] \quad \text{(SE2)}$$

The coefficients in equation (SE1) are determined from observation of surface elevation, surface $\delta^{18}O_{ice}$ and surface temperature on the Greenland ice sheet in the Present Interglacial, the Holocene, and calibration to the observed borehole temperatures at the deep drill sites[32,66,67]. The value of the coefficients are $d\delta^{18}O_{ice}/dS = 0.0062 \pm 0.003$ ‰/m, $d\delta^{18}O_{ice}/dL = 0.48 \pm 0.03$ ‰/Lat Degree and $dT/d\ \delta^{18}O_{ice} = 2.1 \pm 0.2$ K/‰. The stable water isotope values represent the mean value of the deposited snow. If the snow is deposited evenly over the year the mean value is a proxy for the mean annual temperature. If the precipitation is mainly deposited during part of a year, the stable water isotope values will be weighed as the precipitation is distributed. As seasonal resolution is not possible to achieve in the Eemian ice due to annual layers thinner than 1 cm and due to diffusion of the isotopes it is not possible directly to measure the seasonal distribution of precipitation. The equation (SE1) cannot directly be transferred to other and different climate periods because the calibration assumes similar distribution of the precipitation and unchanged atmospheric circulation so the source of the moisture is unchanged. The last interglacial, the Eemian, was warmer than the temperatures found in the early warm Holocene period. In climate reconstructions the $dT/d\ \delta^{18}O_{ice}$ gradient has been given values from 1.2 to 3 K/‰[68,69]. Studies using GCM models including the transport of the stable water isotopes inform that under orbital driven warmer climate as was the case at the onset of the Eemian (127-125 kyr BP) summer temperatures where much warmer than the present while winter temperatures where less influenced[30,69,70]. More moisture would arrive in the summer month which would bias the mean $\delta^{18}O_{ice}$ values towards the warmer summer months[30]. This would influence the temperature stable isotope gradient towards increased values when compared to the present[69,70]. When taking into consideration that there is also a gradient of the northern summer insolation in the Holocene and considering large differences in model results and lacking interactive feedback with a changing Greenland ice sheet it is difficult to select a better temperature isotope gradient in the last interglacial than the Holocene relation. Accordingly, we assume that the temperature/isotope gradient in (SE1) is still applicable but we increase its uncertainty to 0.5 K/‰. Note, that the local warming at the site of deposition and thus the temperature isotope gradient used is also corroborated by the melt layer evidence and the independent temperature reconstruction using $\delta^{15}N$.

4. Deformation contrast between glacial and Eemian ice

The CReSIS Radio Echo Sounding (RES) images, obtained through NASA Operation IceBridge[15,16] (http://nidc.og/data/icebridge/index.html), reveal layers close to the bed with a resolution not previously obtained (ftp://data.cresis.ku.edu/data/rds/2011_Greenland_P3/pdf/). In addition to the image from the NEEM deep drilling site, three images from north Greenland were selected to demonstrate that internal layers in the deep ice from the Eemian period and older are more or less always fuzzy, folded, and disturbed. From these images (and many more,) it seems as though the ice from the glacial period flows over a hard layer of ice from the Eemian and deforms differently. As seen in Figure 3, ice crystals in the Eemian ice are 25 mm, 16 times larger than the ice crystals from the above-lying glacial ice, which are typically about 1.5 mm. The small glacial ice crystals are aligned with the c-axis along the vertical direction; however, the big Eemian ice crystals have multiple maxima. The deformational viscosity contrast of the ice is assumed to be of the order 50-100 [21,71-74]. It is proposed that the observed disturbances and overturning folds of the Eemian ice are caused by the different properties of the ice. It should be noted that the disturbed ice at the Greenland ice cores GRIP[75] and GISP2[76] both start at the end of the dated ice, where the age is 105 kyr BP [10]. This is the same age at which disturbances begin to occur in the NEEM ice core.

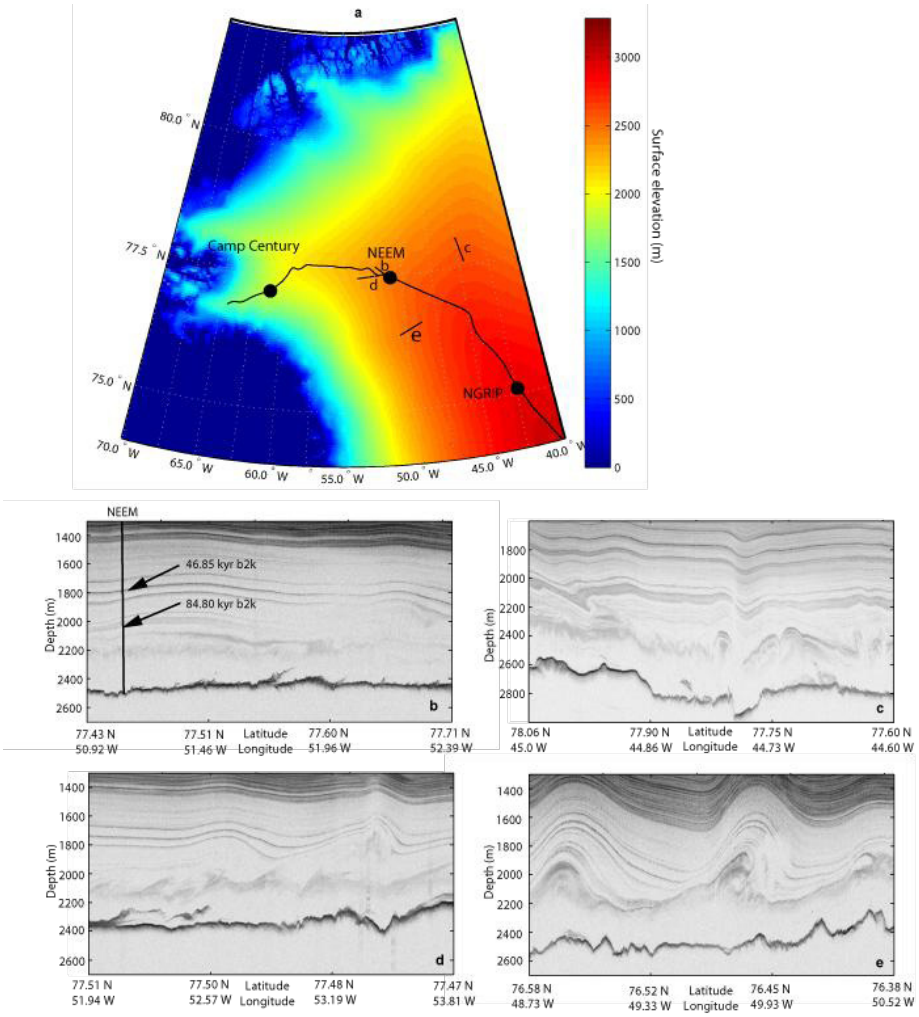

Figure S2. Example of images from NASA Operation IceBridge 2011[15,16]. The CReSIS Radio Echo Sounder (RES) images are enhanced to show deep layers. a) The location of the ice core drill sites and images are shown on the elevation map of northwest Greenland. On the map, the main ice-ridge is also shown as a thin black curve. Image b MCoRDS 20110329_02_028, 48 km is along the ice-ridge flowline at the NEEM ice-core site and only shows results for depths deeper than 1500 m. The RES layers are dated by comparison with the NEEM record, and the fuzzy and disturbed layers can be seen below 2205 m (106 kyr b2k). On images c-e c: MCoRDS 20110329_01_025, 52 km; d: MCoRDS 20110506_01_009, 45 km; e: MCoRDS 20110329_02_020; 52 km, the dated center band located between 1500 and 2000 m on the images and consisting of three layers (centre band: 46.85 kyr b2k) can be identified. In addition, the 84.80 kyr b2k layer at the bottom of the grey band is also discernible. The fuzzy and disturbed layers are always seen below these recognizable layers.

5. Time scale for the NEEM ice

The construction of the time scale for the NEEM ice core for ice deeper than 2017 m can be described by dating the undisturbed part (A), the disturbed part younger than 122 kyr BP before year 2000 (b2k) (B) and the disturbed ice older than 122 kyr b2k (C). Below 2432 m no attempt to date the ice has been made.

A: Based on the Electrical Conductivity Measurements (ECM) 740 match points have been identified between the NEEM record and the NGRIP record which is dated by the GICC05 model-extended time scale. The match starts at the surface and reaches to the depth of 2203.597 m (108.17 kyr b2k). GICC05modelext is available from www.iceandclimate.dk/data. A last tie point below 2203.597 (GIC05 ice age 108.17 kyr b2k) has been added here.

B: Based on the global $\delta^{18}O_{atm}$ and CH_4 records from NGRIP and EDML and finally the nearby NGRIP $\delta^{18}O_{ice}$ the trajectory of the NEEM records can be matched back to the oldest age of the NGRIP record of 122 kyr b2k (NEEM depth 2398.2 m). The gas tie points between NGRIP GICC05 and EDML [6,12] are used to connect the NGRIP and EDML records.

C: The disturbed part of the NEEM ice core between 2398.2 m and 2432.2 m is matched to the NGRIP and EDML global records of $\delta^{18}O_{atm}$ and CH_4 [6,9,10,81,82] as described on the next page.

	A: Undisturbed ice		B: Disturbed ice On NGRIP time scale		C: Disturbed ice Older than NGRIP ice	
	NGRIP GICC05 extended [77-80] (www.iceandclimate.dk/data) NGRIP-EDML gas tie points[6] NGRIP delta age [6] NEEM-NGRIP ice tie points (unpublished) EDML ice age and delta age[4] Assumed: NEEM delta age = 0.20/0.22*NGRIP delta age Note: A last tie point below 2203.597 (GIC05 ice age 108.174 kyr b2k) has been added here.		NGRIP GICC05 extended [77-80] (www.iceandclimate.dk/data) NGRIP-EDML gas tie points[6] NGRIP delta age [6] NEEM-NGRIP ice tie points (unpublished) EDML ice age and delta age[4] Assumed: NEEM delta age = 0.20/0.22*NGRIP delta age NEEM dated by trajectory fit to EDML gas ages (Figures S3, S4)		EDML ice age and delta age[4] Assumed: NEEM delta age = 0.20/0.22*346.9 years (min NGRIP delta age in the warm Eemian ice [6]) NEEM dated by trajectory fit to EDML gas ages. (Figures S3, S4)	
	GICC05	EDML1	GICC05	EDML1	GICC05	EDML1
NEEM						
Start depth	2017.0 m		2204.5 m		2398.2 m	
Stop depth	2204.5 m		2398.2 m		2432.2 m	
Start ice age	74.48 kyr b2k	73.33 kyr BP	108.40 kyr b2k	Traj. Fit + delta age 106.90 kyr BP	Not available	Traj. Fit + 0.20/0.22*346.9 122.96 kyr BP
Stop ice age	108.27 kyr b2k	106.87 kyr BP	122.07 kyr b2k	Traj. Fit + delta age 122.87 kyr BP		Traj. Fit + 0.20/0.22*346.9 128.62 kyr BP
Start gas age	73.47 kyr b2k	72.31 kyr BP	107.99 kyr b2k	Traj. Fit 106.50 kyr BP		Traj. Fit 122.64 kyr BP
Stop gas age	107.91 kyr b2k	106.50 kyr BP	121.75 kyr b2k	Traj. Fit 122.55 kyr BP		Traj. Fit 128.30 kyr BP
NGRIP						
Start depth	2551.4 m		2939.1 m		Not available	
Stop depth	2939.0 m		3082.7 m			
Start ice age	74.48 kyr b2k	73.33 kyr BP	108.39 kyr b2k	106.88 kyr BP		
Stop ice age	108.27 kyr b2k	106.87 kyr BP	122.14 kyr b2k	122.94 kyr BP		
Start gas age	73.36 kyr b2k	72.21 kyr BP	107.97 kyr b2k	106.47 kyr BP		
Stop gas age	107.87 kyr b2k	106.46 kyr	121.79 kyr b2k	122.59 kyr BP		
EDML						
Start depth	1878.1 m		2227.8 m		2337.3 m	
Stop depth	2227.7 m		2336.8 m		2366.3 m	
Start ice age	74.51 kyr b2k	73.36 kyr BP	109.14 kyr b2k	107.63 kyr BP	Not available	123.32 kyr BP
Stop ice age	109.03 kyr b2k	107.62 kyr BP	122.42 kyr b2k	123.22 kyr BP		128.30 kyr BP
Start gas age	73.36 kyr b2k	72.21 kyr BP	107.97 kyr b2k	106.47 kyr BP		122.69 kyr BP
Stop gas age	107.87 kyr b2k	106.46 kyr BP	121.79 kyr b2k	122.59 kyr BP		127.81 kyr BP

*Tabel ST1. Table listing the ice and gas ages for the NEEM record. The three parts A,B and C of the NEEM ice core are dated on the EDML1 and the GICC05 time scales when available. The EDML1 times scale is in 1000 years before AD1950 (*kyr BP*) while the GICC05 time scale is in 1000 years before AD2000 (*kyr b2k*).*

The NEEM ice below 2204.5 m is disturbed and a time scale has been made based on the match to NGRIP and EDML $\delta^{18}O_{atm}$ and CH_4 and when possible guided by the NGRIP $\delta^{18}O_{ice}$ (part B and C)

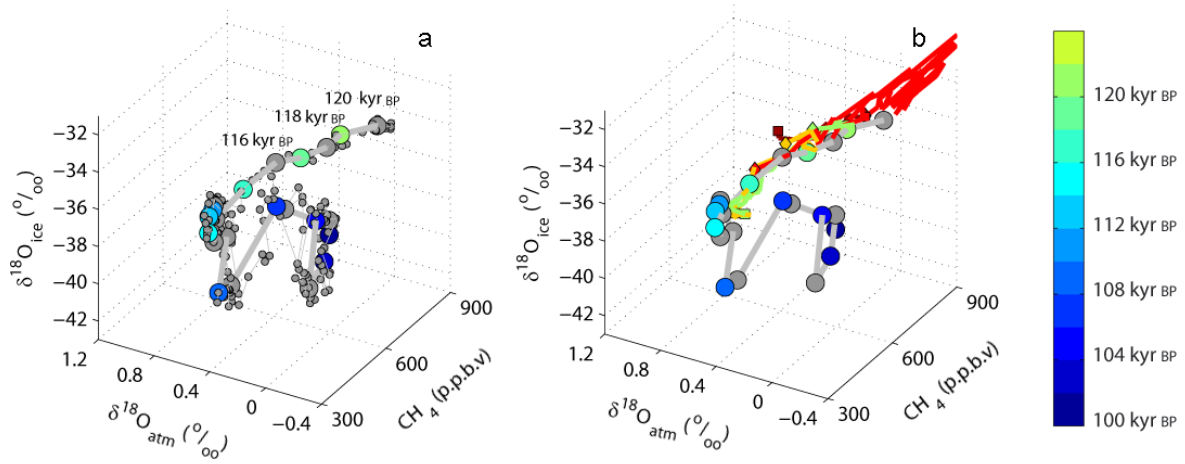

Figure S3. Matching the NEEM data to NGRIP. a) NGRIP trajectory for ice older than 100 kyr BP *in the* $\delta^{18}O_{atm}$, CH_4 $\delta^{18}O_{ice}$ *space. The gas ages of* $\delta^{18}O_{atm}$ *and* CH_4 *are translated to the EDML gas ages by the gas tie points in* [6]*. Markers for each 1000 years on the EDML1 time scale are interpolated onto the trajectory. b) The NEEM trajectory is added to the space using the colored zones as described in Figure 1 (xy projection on Figure S4)*

From the NGRIP trajectory on figure S3a it can be seen that the arm with ice older than 114 kyr BP stands alone and is easy to recognize due to the increasing values of CH_4 and $\delta^{18}O_{ice}$. When the NEEM trajectory for the zones 2-5 are added it is clearly seen that zones 2 and 3 (orange and green) are along the 114-122 kyr BP NGRIP trajectory. The lowest values of the CH_4 record in zone 4 coincide with the NGRIP CH_4 values and can be considered to be uncorrupted. Observations from zone 5 (dark red) are not found along the 114-122 kyr BP NGRIP trajectory. There is also no NEEM data along the NGRIP trajectory 108 kyr BP to 114 kyr BP .

To compare with the longer EDML time scale a x-y projection of the trajectories in the $\delta^{18}O_{atm}$, CH_4 plane is shown on Figure S4. The NGRIP and EDML trajectories are those used by [6] to determine the gas tie points between the NGRIP and EDML records. When the EDML trajectory is shifted CH_4 50 ppbv towards higher values the NGRIP and EDML trajectories fall on top of each other (Figure S4b). The interpolar gradient of methane in the present interglacial, the Holocene, (0-11.7 kyr b2k) is discussed in[53,83] and reaches values of 50 ppbv in the early Holocene. While the

glacial values of the interpolar gradient is lower, the proposed Eemian interpolar gradient of 50 ppbv is in agreement with the gradient of the early Holocene. The NEEM trajectory from zone 5 (dark red) follows the EDML trajectory back to a 128.3 kyr BP gas age.

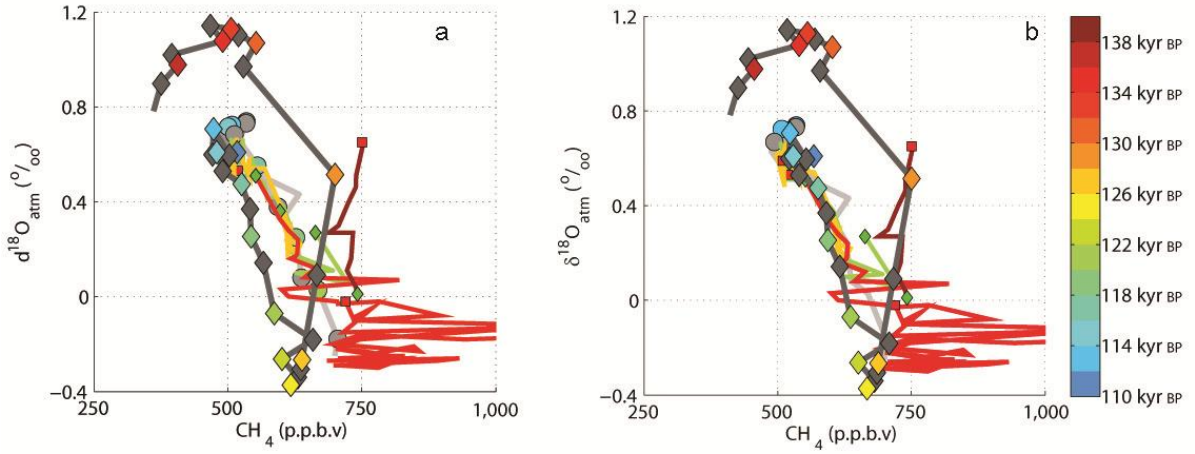

Figure S4 Matching the NEEM data to EDML and NGRIP. a) The x-y plane projection of the data shown on Figure S3b. The NGRIP trajectory (light grey) has 1000 year marks (circles) color coded by the colorbar. The EDML trajectory (dark grey) with 1000 year marks (diamonds). The NGRIP and EDML trajectories are those used by (Capron, 2010) to tie NGRIP and EDML together. b) the EDML trajectory is shifted by 50 ppbv on the CH_4 axis towards higher values to match the NGRIP trajectory to account for an interhemispheric gradient in CH_4.

The CH_4 spikes in zone 4 make the comparison to CH_4 from other ice cores more complicated to interpret. The most robust globally-homogenous parameter is the $\delta^{18}O_{atm}$ records. On Figure S5 the NEEM $\delta^{18}O_{atm}$ values are plotted against those from NGRIP (light grey) and EDML (dark grey). The NEEM $\delta^{18}O_{atm}$ show a good fit to those from EDML and NGRIP.

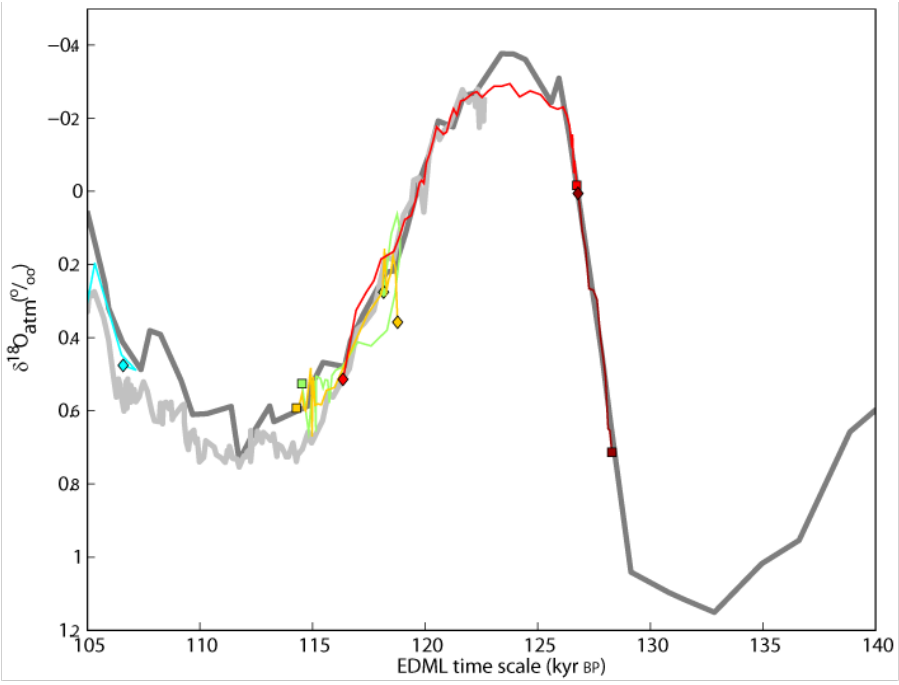

Figure S5 NEEM $\delta^{18}O_{atm}$ compared to NGRIP and EDML $\delta^{18}O_{atm}$. The fitted NGRIP data in the colored zones 1-5 compared to the NGRIP (light grey) and the EDML (dark grey) on the EDML1 age scale.

6. The zone 4 with surface melt

The spikes in CH_4 and N_2O records between 2264.45m and 2418m are too rapid to be explained by climatic variability. The spikes coincide with low air content in the ice and this points strongly to surface melt. Surface melt lowers the air content in the sample measured and favors in situ production of CH_4 and N_2O in the ice. Figure S6 demonstrates the strong correlation between the high concentrations of CH_4 and N_2O and low air content. The low air content is understood to be caused by inclusions of melt layers in which no air bubbles are found. As discussed later, the air content is also dependent on changing insolation but the melt-induced variations in zone 4 are dominating. Measurements of the isotope $\delta^{15}N$ in the air concentration of N_2O allows a second and independent evaluation of the depositional surface temperatures at NEEM. The $\delta^{15}N$ values do not seem to be strongly influenced by the surface melt as the variability of $\delta^{15}N$ in the melt zone is similar to that seen in the other zones. $\delta^{15}N$ has a constant value in the atmosphere and the changes observed in the ice cores are believed to be caused by gravitational and thermal fractionation in the firn layer[22,84-87]. The model for gravitational fractionation[22] assumes that the levels of $\delta^{15}N$ are

proportional to the DCH (diffusive column height) which is also the LID (lock-in-depth) and inversely proportional to the mean firn temperature (T_{mean})

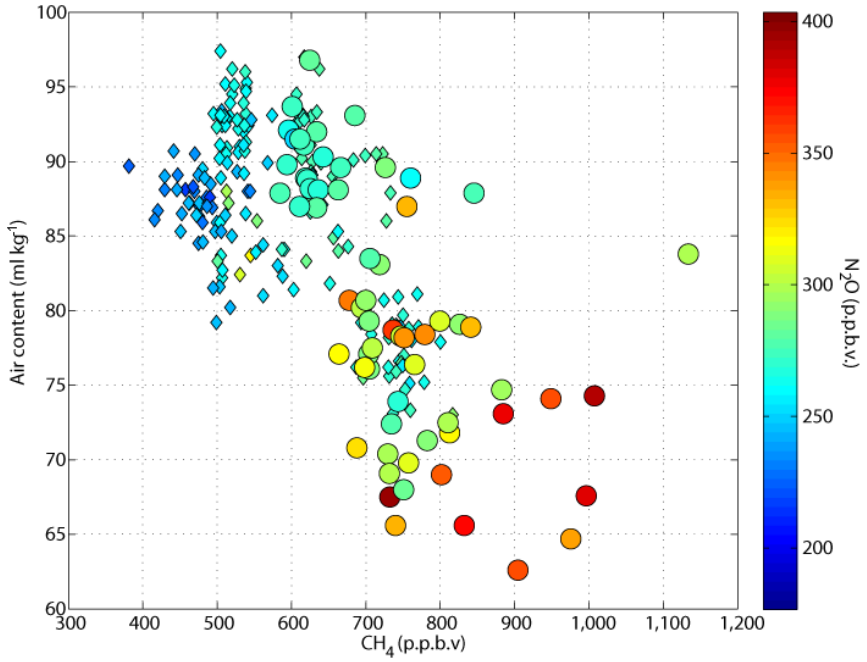

Figure S6 Scatter plot of the CH_4 concentrations against the air content. The data points are colored by their N_2O concentrations shown on the color bar. The measurements are those shown on Figure 1 from a depth of 2201.7m to 2518.5m. The data points from the depth zone 2264.5 m to 2418 m, the zone 5 with CH_4 and N_2O spikes, are marked with large circles while the rest are marked with smaller diamonds.

The $\delta^{15}N$ measurements of ice older than 100 kyr BP are shown in Figure S7. In addition 5 samples from the depths 396-416 m and ages 1846 – 1957 yr b2k have been measured, defining the mean present level to be 0.34 ‰. The mean annual temperature at NEEM at present is -29 ^{o}C. In the melt zone the $\delta^{15}N$ level drops to 0.25 ‰ and application of the Goujon model[22] suggests a warming of the top of the firn layer by 5 ^{o}C compared to the present temperatures. The $\delta^{15}N$ levels in the zone with CH_4 spikes therefore suggests annual surface temperatures warmer than the present and they are thus supportive of surface melt 127-118.3 kyr BP.

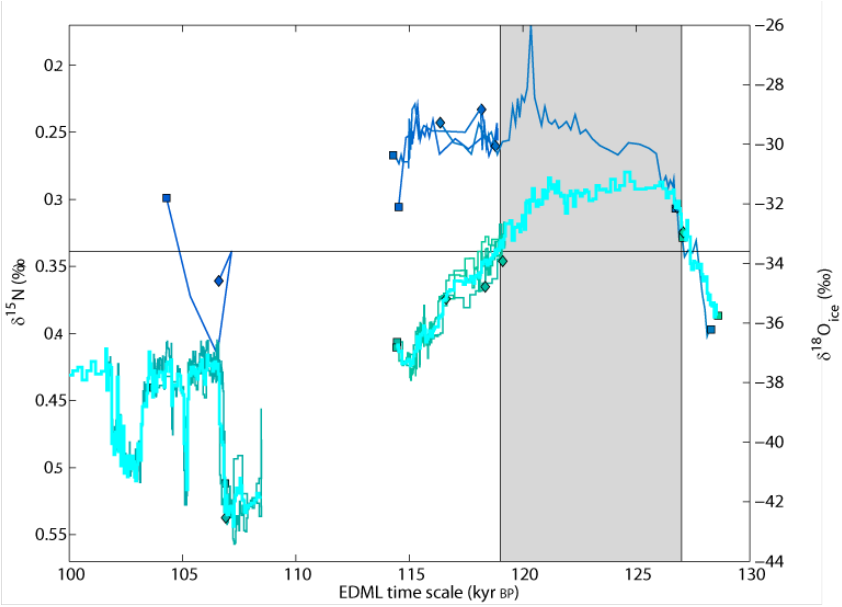

Figure S7 Plot of NEEM $\delta^{15}N$. Plot of $\delta^{15}N$ (blue colors) on a reverse scale on the left and $\delta^{18}O_{ice}$ (cyan,green colors) on the scale to the right for the period 130-100 kyr BP *(EDML1 time scale). The zone with CH_4 spikes (127-118.3* kyr BP*) is shaded grey. The present level of $\delta^{15}N$ (0.34 ‰) and $\delta^{18}O$ (-33.6 ‰) are marked by a black line.*

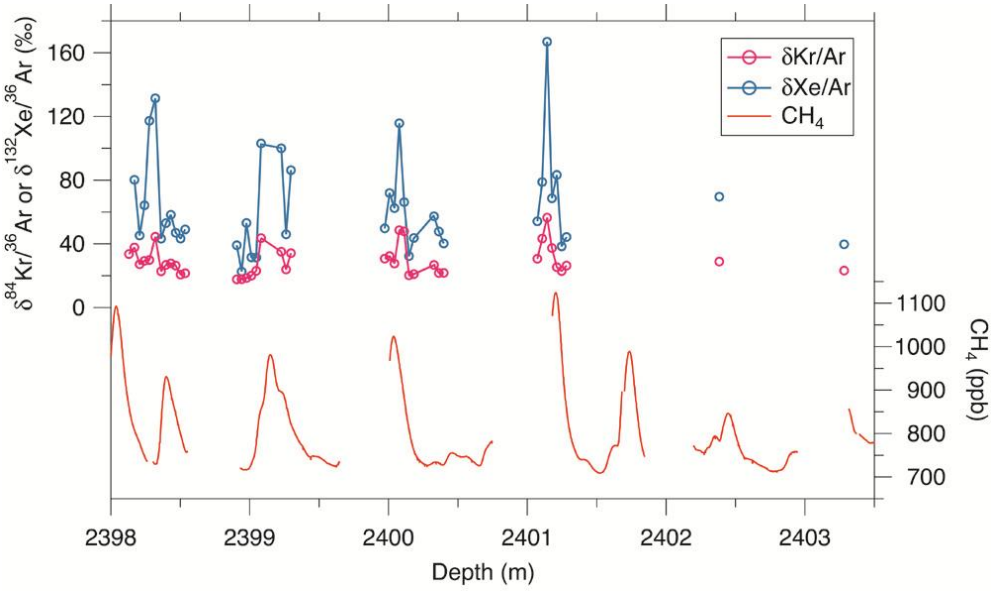

Figure S8 NEEM noble gasses over CH_4 spikes. Measurements of Xe/Ar (132/36, blue) and Kr/Ar (84/36, pink) shown together with CH_4 (red) over some of the CH_4 spikes at the depths 2398-2404m

Measurements of the noble gasses Xe/Ar and Kr/Ar over some of the CH_4 spikes show a strong correlation with the increased levels of the CH_4 spikes and this again points towards melt layers and surface melt. A study of noble gasses has also been made on shallow ice from Dye3 in South Greenland from 115 m and 144m depths where melt layers are visible[88], confirming the relationship between increased levels of the noble gasses and CH_4 levels in melt layers.

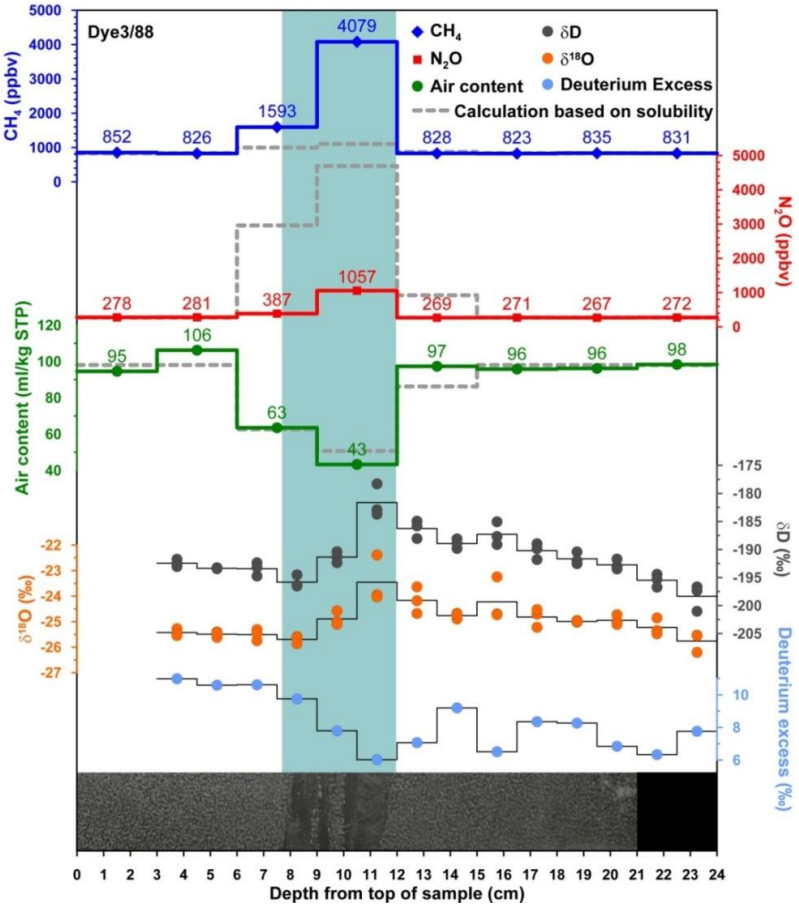

Figure S9. Analysis of a clearly visible melt layer in ice from Dye3 at a depth of 88 m. At the University of Bern, consecutive samples of 3 cm length are measured for CH_4, N_2O, and air content and consecutive samples of 1.5 cm length are measured for δD and $\delta^{18}O_{ice}$, from where deuterium excess is calculated. The melt layer is indicated by the blue shading and the picture of the ice sample at the bottom of the plot. The dashed grey lines show the expected values for CH_4, N_2O, and air content under the assumption that solubility is the only mechanism affecting the gas concentrations in the melt layer.

Existence of CH_4, N_2O, and air content spikes caused by melt layers in the Eemian ice is supported by similar behavior in the near surface ice from the warmer Dye3 site (south Greenland, annual mean surface temperature -21°C), where measurements are made over a 3 cm thick and clearly visible melt layer (Figure S9). Within the melt layer, the concentrations strongly increase to >4000 ppbv for CH_4 and >1000 ppbv for N_2O, while the air content decreases by about 60%. The isotopic composition of the ice does not show spikes within the melt layer, the observed changes in δD, $\delta^{18}O$, and deuterium excess may instead be related to annual cycles. The expected changes in air content, CH_4, and N_2O based on solubility effects only are also calculated. For that purpose the fraction of liquid water which corresponds to the missing fraction of air content is estimated and it is further assumed that the liquid phase was in equilibrium with the atmosphere at that time.

To calculate the equilibrium gas concentrations of the water phase the Henry constants of the respective gases at 0°C are used. Since N_2O is more soluble than CH_4, N_2, and O_2, the liquid phase is enriched with N_2O and only marginally with CH_4. During the refreezing step it is assumed that the total gas content of the liquid phase becomes trapped in the ice phase. From the comparison of the measured values with these modeled values (see Figure S9) it is apparent that the elevated CH_4 concentrations cannot be explained by physical processes alone and must therefore originate from biological or chemical processes, thus in situ production. In contrast, the elevated N_2O concentrations are within the range of the modeled values and could thus be explained by the solubility effect alone, however, it cannot be excluded that in situ production also contributes to the observed N_2O spike.

7. Greenland air content and relation to elevation changes

The air content in the trapped air bubbles in the ice core depend on the atmospheric pressure at the depositional site and is one of the most direct methods available for reconstructing the past elevation changes of the ice core sites[49,89,90]. Newer studies suggest that the air content also strongly depend on the summer insolation because the trapping of the air bubbles in the firn depend on the temperature gradient through the first 70-100m of the firn[22,28,31,50,86,91,92] The existing air content measurements from the Greenland ice cores in the present interglacial, the Holocene 11.7 kyr b2k to present, are used to establish a relationship between the observed air content, the elevation changes and the northern hemisphere summer insolation. The relationship will be used on the NEEM observation from the last interglacial, the Eemian, 128.5 – 114 kyr BP where summer insolation changes are stronger than during the present interglacial.

Assuming the depostitional surface elevations for GRIP, Camp Century and NEEM [17,32,35], the 75 deg N summer insolation[29] and the depositional stable water isotopes from the ice core measurements are known the observed air content data from all three locations (GRIP, NEEM and Camp Century (both old and new observations)) are fitted to the equation:

$$\mathrm{Air}(time) - Air_{present}^{site} = \beta\left[Ins(time) - Ins_{present}\right] + \gamma\left[Sur(time) - Sur_{present}^{site}\right] \quad \text{(SE3)}$$

In the Monte Carlo inversions the unknowns (red) are the present values of the air content ($Air_{present}^{site}$) at GRIP, NEEM and Camp Century new and old, β and γ (6 model parameters). The present value of the northern insolation for the four summer months is $Ins_{present}$ = 428.06 W/m^2 and the present values of the $\delta^{18}O_{ice}$ are taken as the mean over the last 1000 years (GRIP: -35.31‰, NEEM: -33.60 ‰ and CC: -29.20 ‰). In Figure S10 histograms of the accepted values of model parameters (present values of the air content content ($Air_{present}^{site}$) β and γ) are show to the left while a comparison of the observed and modelled air contents for the four data sets (GRIP, NEEM, CC, CC08) are shown to the right. It can be seen that at GRIP the insolation component of the air content signal is 80% at the Holocene climatic Optimum, 8 kyr b2k, while it is 50% at NEEM and 40% at Camp Century because there occur larger elevation changes away from the center of the ice sheet. The difference in elevation changes and, thus, the varying relative contribution of the summer insolation leads to a very confident determination of the effect of the insolation in the equation SE3.

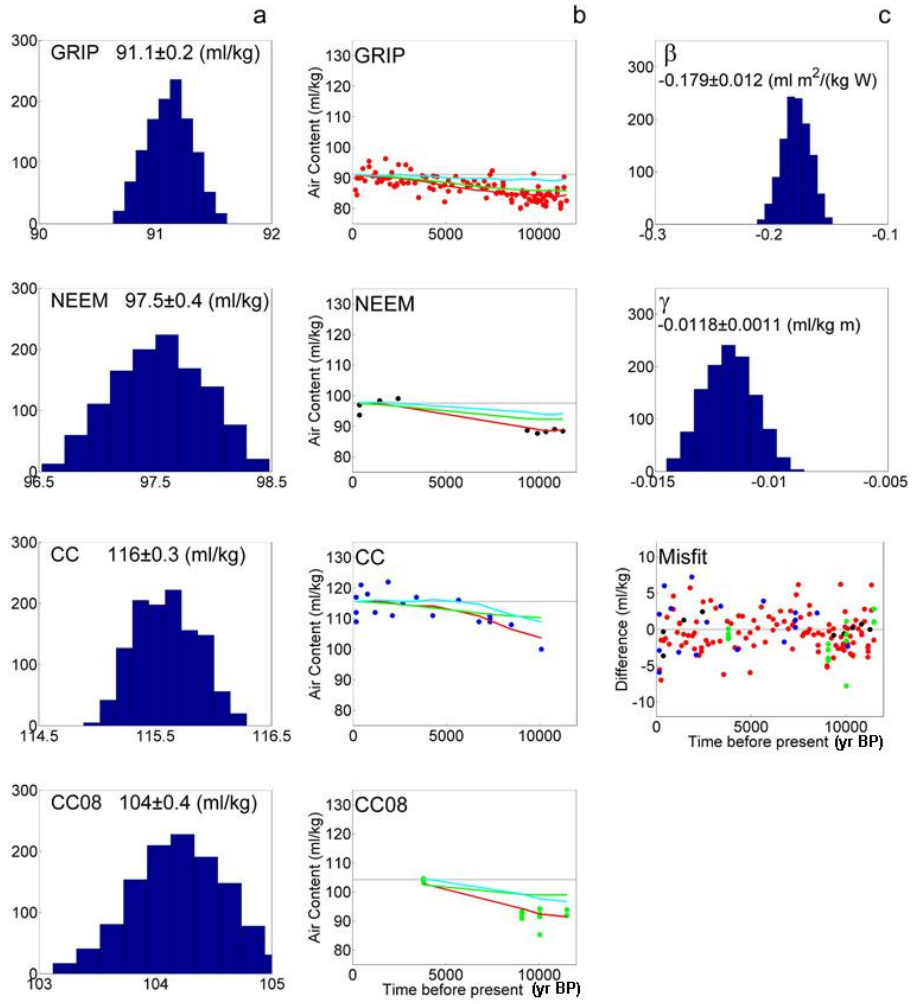

Figure S10. Monte Carlo fit of observed air content. a) Histograms of the Monte Carlo simulations of the present air contents, $Air^{site}_{present}$ for GRIP, NEEM , Camp Century old (CC) and Camp Century new (CC08). The mean values and the standard deviation of the present air content values are shown in each frame and listed in table ST2. b) The modelled air content (Equation SE5) compared with the observed air content data for GRIP(red dots), NEEM (black dots) , Camp Century old (CC) (blue dots) and Camp Century new (CC08) (green dots) as functions of time. The modeled air content (red curves) are the sum of the insolation component(green curves) and the surface elevation change component (cyan curves) when added to the present air content values (grey line). c) From the top, the histograms of the Monte Carlo simulations of the β and the γ constants in the aircontent equation (SE3). The mean value and the standard deviation of β and γ are shown in each frame. The bottom frame shows the misfit of the modeled air content values when compared to the observed air content values from b).

	Value	Standard Error	Units
$Air_{present}^{GRIP}$	91.12	0.19	ml/kg
$Air_{present}^{NEEM}$	97.53	0.39	ml/kg
$Air_{present}^{CC}$	115.60	0.27	ml/kg
$Air_{present}^{CCO8}$	104.20	0.40	ml/kg
β	-0.179	0.012	(ml m^2)/(kg W)
γ	-0.0118	0.0011	ml/(kg m)

Tabel ST2 Values of the Monte Carlo determined model parameters for equation SE3.

Equation SE3 will be used together with the NEEM air content measurements to quantify the altitude changes during the Eemian, where the insolation is known to have very large variations. The past surface elevation Sur(time) is the sum of the flow induced elevation change and the elevation change of the ice core site.

$$Sur(time) = Upstream(time) + Sur^{NEEM}(time) \quad \text{(SE4)}$$

Combining equations SE3 and SE4 leads to:

$$\left[Sur^{NEEM}(time) - Sur_{present}^{NEEM}\right] = \quad \text{(SE5)}$$

$$\left\{\left[Air(time) - Air_{present}^{NEEM}\right]/\gamma - Upstream(time) - \quad \beta\left[Ins(time) - Ins_{present}\right]/\gamma\right\}$$

$Sur_{present}^{NEEM}$, $Air_{present}^{NEEM}$, γ , β and the past summer insolation are known and the past elevation changes $Sur^{NEEM}(time)$ of the NEEM site can be determined from the air content measurements. The equation SE5 is used to determine the elevation change of the NEEM site during the Eemian as shown in Figure 4.

8. Additional References

51 *Dansgaard, W., Johnsen, S. J., Clausen, H. B. & Gundestrup, N. Stable isotope glaciology. Meddelelser om Grønland* ***197****, 1-53 (1973).*

52 *Epstein, S. & Mayeda, T. Variation of the 18-O content of waters from natural sources. Geochimica et Cosmochimica Acta* ***4****, 213-224 (1953).*

53 *Chappellaz, J. et al. Changes in the atmospheric CH_4 gradient between Greenland and Antarctica during the Holocene. Journal of Geophysical Research* ***102****, 15987-15997 (1997).*

54 *Flückiger, J. et al. N_2O and CH_4 variations during the last glacial epoch: Insight into global processes. Global Biogeochemical Cycles* ***18****, GB1020, doi:1010.1029/2003GB002122 (2004).*

55 *Schilt, A. et al. Atmospheric nitrous oxide during the last 140 000 years. Earth Planet. Sc. Lett.* ***300****, 33–43 (2010).*

56 *Spahni, R. et al. Atmospheric methane and nitrous oxide of the late Pleistocene from Antarctic ice cores. Science* ***310****, 1317-1321, doi:10.1126/science.1120132 (2005).*

57 *Landais A, S.-L. H., Guillevic M, Masson-Delmotte V, Vinther B, Winkler R. Triple isotopic composition of oxygen in surface snow and water vapor at NEEM (Greenland). Geochimica et Cosmochimica Acta* ***77****, 304-316, doi:10.1016/j.gca2011.11.022 (2011).*

58 *Schwander, J. in Dahlem Konference: The Environmental Record in Glaciers and Ice Sheets Physical, Chemical, and Earth Sciences Research Report 8 (eds H. Oeschger & C.C Langway, Jr.) 53-67 (John Wiley, 1989).*

59 *Lipenkov, V., Candaudap, F., Ravoire, J., Dulac, E. & Raynaud, D. A new device for the measurement of air content in polar ice. Journal of Glaciology* ***41****, 423–429 (1995).*

60 *Martinerie, P., Lipenkov, V. Y. & Raynaud, D. Correction of air-content measuremnts in polar ice for effects of cut bubbles at the surface of the sample. Journal of Glaciology* ***36****, 299-303, doi:10.3189/002214390793701282 (1990).*

61 *Robinson, A., Calov, R. & Ganopolski, A. Greenland Ice Sheet model parameters constrained using simulations of the Eemian Interglacial. Clim. Past.* ***7****, 381-396, doi:10.5194/cpd-6-1551-2010 (2011).*

62 *Buchardt, S. L. Basal melting and Eemian ice along the main ice ridge in northern Greenland, University of Copenhagen, (2009).*

63 *Steen-Larsen, H.C et al. nderstanding the climatic signal in the water stable isotope records from the NEEM shallow firn/ice cores in northwest Greenland. Journal of Geophysical Research Atmospheres* ***116****, 20, doi:10.1029/2010JD014311 (2011).*

64 *Hvidberg, C. S., Larsen, L. B., Dahl-Jensen, D. & Buchardt, S. L. Surface movement and elevation change at the NEEM deep drilling site,North Greenland, 2007-2011. Geophysical Research Abstracts* ***14*** *(2012).*

65 *Bintanja, R., van de Wal, R. S. W. & Oerlemans, J. A new method to estimate ice age temperatures. Climate Dynamics* ***24****, 197-211, doi:10.1007/s00382-004-0486-x (2005).*

66 *Johnsen, S. J., Dansgaard, W. & White, J. W. C. The origin of Arctic precipitation under present and glacial conditions. Tellus B* ***41****, 452-468 (1989).*

67 *Johnsen, S., Dahl-Jensen, D., Dansgaard, W. & Gundestrup, N. Greenland palaeotemperatures derived from GRIP bore hole temperature and ice core isotope profiles. Tellus B* ***47****, 624-629 (1995).*

68 *Cuffey, K. M. & Marshall, S. J. Substantial contribution to sea-level rise during the last interglacial from the Greenland ice sheet. Nature* ***404****, 591-594 (2000).*

69 *Masson-Delmotte V, B. P., Hoffmann G, Jouzel J, Kageyama M, Landais A, Lejeune Q, Risi C, Sime L, Sjolte J, Swingedouw D, Vinther B. Sensitivity of interglacial Greenland temperature and δ18O: ice core data, orbital and increased CO2 climate simulations. Climate of the Past* ***7****, 1041-1059, doi:10.5194/cp-7-1041-2011 (2011).*

70 *Sjolte J, H. G., Johnsen SJ, Vinther BM, Masson-Delmotte V, Sturm C. Modeling the water isotopes in Greenland precipitation 1959–2001 with the meso-scale model REMO-iso. Journal of Geophysical REsearch Atmospheres* ***116****, 22, doi:10.1029/2010JD015287 (2011).*

71 *Dahl-Jensen, D., Thorsteinsson, T., Alley, R. & Shoji, H. Flow properties of the ice from the Greenland Ice Core Project ice core: The reason for folds? Journal of Geophysical Research* ***102****, 26831-26840 (1997).*

72 *Budd, W. F. & Jacka, T. H. A review of ice rheology for ice sheet modelling. Cold Regions Science and Technology* ***16****, 107-144 (1989).*

73 *Alley, R. B. Fabric in polar ice sheets: Development and prediction. Science* ***240****, 493-495 (1988).*

74 *Alley, R. B., Grow, A. J. & Meese, D. A. Mapping c-axis fabrics to study physical processes in ice. Journal of Glaciology* ***41****, 197-203 (1995).*

75 *Greenland Ice-Core Project (GRIP) Members. Climate instability during the last interglacial period recorded in the GRIP ice core. Nature* ***364****, 203-207 (1993).*

76 *Grootes, P. M., Stuiver, M., White, J. W. C., Johnsen, S. J. & Jouzel, J. Comparison of oxygen isotope records from the GISP2 and GRIP Greenland ice cores. Nature* ***366****, 552-554 (1993).*

77 *Andersen, K. K. et al. The Greenland Ice Core Chronology 2005, 15-42 ka. Part 1: constructing the time scale. Quaternary Science Reviews* ***25****, 3246-3257 (2006).*

78 *Rasmussen, S. O. et al. A new Greenland ice core chronology for the last glacial termination. Journal of Geophysical Research* ***111****, D06102, doi:06110.01029/02005JD006079 (2006).*

79 *Svensson, A. et al. The Greenland Ice Core Chronology 2005, 15-42 ka. Part 2: comparison to other records. Quaternary Science Reviews* ***25****, 3258-3267 (2006).*

80 *Vinther, B. M. et al. A synchronized dating of three Greenland ice cores throughout the Holocene. Journal of Geophysical Research* ***111****, D13102, doi:13110.11029/12005JD006921 (2006).*

81 *Capron E, L. A., Chappellaz J, Schilt A, Buiron D, Dahl-Jensen D, Johnsen SJ, Jouzel J, Lemieux-Dudon B, Loulergue L, Leuenberger M, Masson-Delmotte V, Mayer H, Oerter H, B Stenni. Millennial and sub-millennial scale climatic variations recorded in polar ice cores over the last glacial period. Clim. Past.* ***6****, 135-183, doi:10.5194/cpd-6-135-2010 (2010).*

82 *Landais, A. et al. Evidence for stratigraphic distortion in the Greenland Ice Core Project (GRIP) ice core during Event 5e1 (120 kyr BP) from gas isotopes. Journal of Geophysical Research* ***109****, D06103, doi:06110.01029/02003JD004193 (2004).*

83 *Brook, E. J., Harder, S., Severinghaus, J., Steig, E. J. & Sucher, C. M. On the origin and timing of rapid changes in atmospheric methane during the last glacial period. Global Biogeochemical Cycles* ***14****, 559-572 (2000).*

84 *Landais, A. et al. Quantification of rapid temperature change during DO event 12 and phasing with methane inferred from air isotopic measurements. Earth and Planetary Science Letters* ***225****, 221-232 (2004).*

85 *Landais, A. et al. The glacial inception as recorded in the NorthGRIP Greenland ice core: Timing, structure and associated abrupt temperature changes. Climate Dynamics* ***26****, 273-284 (2006).*

86 *Kobahi T, K. K., Severinghaus JP, Barnola JM, Nakaegawa T, Vinther BM, Johnsen SJ, Box JE. High variability of Greenland surface temperature over the past 4000 years estimated from trapped air in an ice core. Geophysical Research Letters* ***38****, 6, doi:10.1029/2011GL049444 (2011).*

87 *Kobashi, T. S., J.P. Barnola, J.M. 4 ± 1.5 °C abrupt warming 11,270 yr ago identified from trapped air in Greenland ice. Earth and Planetary Science Letters* ***268****, 397-407, doi:10.1016/j.epsl.2008.01.032 (2008).*

88 *Headly, M. A. Krypton and Xenon in Air Trapped in Polar Ice Cores: Paleo-atmospheric Measurements for Estimating Past Mean Ocean Temperature and Summer Snowmelt Frequency. PhD dissertation, University of California San Diego, 229 pp. (2008).*

89 *Raynaud, D. & Lorius, C. Climatic Implications of Total Gas Content in Ice at Camp Century. Nature* ***243****, 283-284, doi:10.1038/243283a0 (1973).*

90 *Herron, S. L. & Langway, C. C. Derivation of paleoelevations from total air content of two deep Greenland ice cores. IAHS. Publication* ***170****, 283-295 (1987).*

91 *Trudinger, C. M. et al. Modeling air movement and bubble trapping in firn. Journal of Geophysical Research* ***102****, 6747-6764 (1997).*

92 *Herron, M. M. & Herron, S. L. Past atmospheric environments revealed by polar ice core studies. Hydrological Sciences-Journal-des Sciences Hydrologiques* ***28****, 139-153 (1983).*